Applications of Mathematics

Vladimír Janovský

Analysis of pattern formation using numerical continuation

Applications of Mathematics, Vol. 67 (2022), No. 6, 705–726

Persistent URL: http://dml.cz/dmlcz/151053

67 (2022) APPLICATIONS OF MATHEMATICS No. 6, 705–726

ANALYSIS OF PATTERN FORMATION USING NUMERICAL CONTINUATION

Vladimír Janovský, Praha

Received May 30, 2021. Published online May 2, 2022.

Abstract. The paper deals with the issue of self-organization in applied sciences. It is particularly related to the emergence of Turing patterns. The goal is to analyze the domain size driven instability: We introduce the parameter L, which scales the size of the domain. We investigate a particular reaction-diffusion model in 1-D for two species. We consider and analyze the steady-state solution. We want to compute the solution branches by numerical continuation. The model in question has certain symmetries. We define and classify them. Our goal is to calculate a global bifurcation diagram.

Keywords: pattern formation; reaction-diffusion model; Turing instability; diffusion-driven instability; bifurcation

MSC 2020: 35K57, 35B36, 92C15, 34B24

1. Introduction

The paper deals with the issue of self-organization in developmental biology, in particular "morphogenesis", see review in [2]. In his key work [20] Turing formulated the principles of pattern formation in reaction-diffusion systems. In particular, the mechanism of reaction-diffusion systems involving two species, see [17]. We speak of diffusion-induced instability. For the theory of biological pattern formation, see [7]. In particular, [13] discusses receptor-mediated patterning and [14] domain size-dependent instabilities. For a theory of Turing pattern instabilities in reaction-diffusion-ODE systems, we refer to [16].

We investigate numerical solutions of reaction-diffusion models. We deal with the steady state solutions. We use numerical continuation to find branches of the solution, see [1], [10]. We use ready made packages [5], [6]. We consider branching solutions. For this, we use the theory of bifurcations [15], [8]. The problems we study have certain symmetries, see [8], [9]. We refer to the equivariant bifurcation theory,

DOI: 10.21136/AM.2022.0126-21

see [9], [4]. For the numerical treatment of symmetry breaking bifurcation points we refer to [3] and [11].

The outline of the paper is as follows: In Section 2, we define the *domain size driven instability*, see [14]. We investigate a particular reaction-diffusion model in 1-D. The aim is to compute the branches of the solution. For this purpose, we use numerical continuation. In following Section 3 we analyze the dispersion equation: We define critical wavelengths. We identify them with the primary bifurcation points. In Section 4 we define and classify the symmetries of the model. Our goal is to compute a global bifurcation diagram. Finally, we compare the numerical continuation with the dynamical simulation. The latter technique is currently used in practice.

2. Pattern formation and numerical continuation

We consider the Turing instability in the context of reaction-diffusion systems for two species $\mathbf{u}$ and $\mathbf{v}$ in a 1-D domain $x \in [0, l]$. The goal of the analysis is the *domain size driven instability*, see [14],

$$\begin{aligned} \mathbf{u}_t &= d_1 \mathbf{u}_{xx} + \overline{f}(\mathbf{u}, \mathbf{v}), \\ \mathbf{v}_t &= d_2 \mathbf{v}_{xx} + \overline{g}(\mathbf{u}, \mathbf{v}) \end{aligned} \tag{2.1}$$

in the domain $0 \leqslant x \leqslant l$. The domain can be scaled to a unit interval $0 \leqslant x \leqslant 1$ if we introduce a parameter L^2. Therefore, we consider

$$\begin{aligned} \mathbf{u}_t &= \frac{d_1}{L^2} \mathbf{u}_{xx} + f(\mathbf{u}, \mathbf{v}), \\ \mathbf{v}_t &= \frac{d_2}{L^2} \mathbf{v}_{xx} + g(\mathbf{u}, \mathbf{v}) \end{aligned} \tag{2.2}$$

in the range $0 \leqslant x \leqslant 1$. Here L is the length of the interval.

We consider Neumann boundary conditions (zero flux)

$$\mathbf{u}_x(0,t) = \mathbf{u}_x(1,t) = 0, \quad \mathbf{v}_x(0,t) = \mathbf{v}_x(1,t) = 0. \tag{2.3}$$

We are looking for *steady states* of the system (2.2) that satisfy conditions (2.3). We assume the existence of a *homogeneous steady state*: There exist $u^* \in \mathbb{R}^1$, $v^* \in \mathbb{R}^1$ such that

$$f(\mathbf{u}(x,0), \mathbf{v}(x,0)) = f(u^*, v^*) = g(\mathbf{u}(x,0), \mathbf{v}(x,0)) = g(u^*, v^*) = 0, \quad 0 \leqslant x \leqslant 1.$$

Note that in this case $\mathbf{u}_{xx} = 0$ and $\mathbf{v}_{xx} = 0$ in the domain $0 \leqslant x \leqslant 1$.

To discretize the above problem, we use the *method of lines*, i.e. semi-discretization in the spatial variable x. We introduce an equidistant mesh on the interval $0 \leqslant x \leqslant 1$,

$$x_j = jh, \quad h = \frac{1}{N+1}, \quad j = 1, \dots, N, \tag{2.4}$$

where N is the number of mesh points. The state variables $\mathbf{u}$, $\mathbf{v}$ are approximated by discrete state variables

$$\mathbf{u} \approx [u_1, \dots, u_i, \dots, u_N]^\top \in \mathbb{R}^N, \quad \mathbf{v} \approx [v_1, \dots, v_i, \dots, v_N]^\top \in \mathbb{R}^N. \tag{2.5}$$

We look for discrete steady states. These depend on the parameter L^2. The problem can be formulated as a system of $2N$ nonlinear algebraic equations depending on the parameter L^2. We put

$$F\colon\ \mathbb{R}^{2N} \times \mathbb{R}^1 \to \mathbb{R}^{2N} \tag{2.6}$$

and search for the roots

$$F(w, L^2) = 0, \quad w \in \mathbb{R}^{2N}, \quad w_i = u_i, \quad w_{N+i} = v_i, \quad i = 1, \dots, N, \tag{2.7}$$

where

$$\begin{aligned}
F_1(w, L^2) &\equiv 2\frac{d_1}{h^2 L^2}(-u_1 + u_2) + f(u_1, v_1) = 0, \\
F_i(w, L^2) &\equiv \frac{d_1}{h^2 L^2}(u_{i-1} - 2u_i + u_{i+1}) + f(u_i, v_i) = 0, \quad i = 2, \dots, N-1, \\
F_N(w, L^2) &\equiv 2\frac{d_1}{h^2 L^2}(u_{N-1} - u_N) + f(u_N, v_N) = 0, \\
F_{N+1}(w, L^2) &\equiv 2\frac{d_2}{h^2 L^2}(-v_1 + v_2) + g(u_1, v_1) = 0, \\
F_{N+i}(w, L^2) &\equiv \frac{d_2}{h^2 L^2}(v_{i-1} - 2v_i + v_{i+1}) + g(u_i, v_i) = 0, \quad i = 2, \dots, N-1, \\
F_{2N}(w, L^2) &\equiv 2\frac{d_2}{h^2 L^2}(v_{N-1} - v_N) + g(u_N, v_N) = 0.
\end{aligned} \tag{2.8}$$

The set (2.7) is called the *solution manifold*. We assume the existence of a homogeneous steady state

$$F(w^*, L^2) = 0, \quad w^* \in \mathbb{R}^{2N}, \quad w_i^* = u^*, \quad w_{N+i}^* = v^*, \quad i = 1, \dots, N. \tag{2.9}$$

Consider the homogeneous state (2.9). This can be parameterized by L, i.e. by the length of the interval. We speak of a branch of *homogeneous steady states*.

Definition 2.1. Consider a particular homogeneous steady state $w^* \in \mathbb{R}^{2N}$, $(L^*)^2 \in \mathbb{R}^1$,

$$F(w^*, (L^*)^2) = 0 \in \mathbb{R}^{2N}, \quad A \equiv F_w(w^*, (L^*)^2), \quad \dim\ker A = 1. \tag{2.10}$$

Let ξ and η be the right and left eigenvectors corresponding to the zero eigenvalue

$$A\xi = 0 \in \mathbb{R}^{2N}, \quad \|\xi\| = 1, \quad A^\top\eta = 0 \in \mathbb{R}^{2N}, \quad \|\eta\| = 1, \quad \eta^\top\xi \neq 0$$

with algebraic multiplicity equal to one. Then the point $(w^*, (L^*)^2) \in \mathbb{R}^{2N+1}$ is called the *primary bifurcation point* of the system (2.6).

The simplicity of the bifurcation point implies the regularity of the bordered Jacobian

$$\det \begin{bmatrix} F_w(w^*, (L^*)^2) & \xi \\ \eta^\top & 0 \end{bmatrix} \neq 0, \tag{2.11}$$

see [10], Chapter 3.

Let $F \in C^1$ be differentiable in the neighborhood $(w^*, (L^*)^2) \in \mathbb{R}^{2N+1}$. Then there exist a vector function $r = r(y, z) \in \mathbb{R}^{2N}$ and a scalar function $h = h(y, z) \in \mathbb{R}^1$ defined on the neighborhood of the origin $y = 0 \in \mathbb{R}^1$, $z = 0 \in \mathbb{R}^1$, such that

$$F(w, L^2) = F(w^* + r, (L^*)^2 + z) = 0 \in \mathbb{R}^{2N} \Leftrightarrow h(y, z) = 0 \in \mathbb{R}^1, \tag{2.12}$$

where $w = w^* + r(y, z)$. The function $h\colon \mathbb{R}^1 \times \mathbb{R}^1 \to \mathbb{R}^1$ defines the *bifurcation equation*. The state variable y is called *observable*. The bifurcation equation is an analytical tool for studying the solution manifold (2.7) in a neighborhood of a simple bifurcation point. For this purpose, we refer to the Lyapunov-Schmidt reduction [8], Chapter VII as a suitable analytical procedure. In the context of finite-dimensional models (e.g. the model (2.8)), we use the numerical Lyapunov-Schmidt reduction [10], Chapter 6. This technique is based on the systematic use of bordered matrices like (2.11). We are able to analyze Taylor expansions of the bifurcation equation in the neighborhood of the origin $y = 0 \in \mathbb{R}^1$, $z = 0 \in \mathbb{R}^1$:

$$\begin{aligned} h(y, z) &= h_y(0, 0)y + h_z(0, 0)z + h_{yy}(0, 0)y^2 + \ldots \in \mathbb{R}^1, \\ r(y, z) &= r_y(0, 0)y + r_z(0, 0)z + r_{yy}(0, 0)y^2 + \ldots \in \mathbb{R}^{2N}. \end{aligned} \tag{2.13}$$

The leading term $h_y(0, 0) \in \mathbb{R}^1$, $r_y(0, 0) \in \mathbb{R}^{2N}$ of the expansion (2.13) is defined by means of the bordered linear system

$$\begin{bmatrix} F_w(w^*, (L^*)^2) & \xi \\ \eta^\top & 0 \end{bmatrix} \begin{bmatrix} r_y(0, 0) \\ h_y(0, 0) \end{bmatrix} = \begin{bmatrix} 0 \in \mathbb{R}^{2N} \\ 1 \in \mathbb{R}^1 \end{bmatrix}. \tag{2.14}$$

For a small given parameter δ, we can approximate the inhomogeneous steady state close to the bifurcation point $(w^*, (L^*)^2)$ as

$$(w^* + \delta r_y(0,0), (L^*)^2). \tag{2.15}$$

It will serve as an initial guess to approximate the whole solution manifold (2.7).

The solution manifold (2.7) consists of implicitly defined curves, namely of the branch of homogeneous steady states (2.9) and of the branch of *inhomogeneous steady states*, emanating from the primary bifurcation point $(w^*, (L^*)^2) \in \mathbb{R}^{2N+1}$. The latter branch consists of pairs $(w, L^2) \in \mathbb{R}^{2N} \times \mathbb{R}^1$,

$$F(w, L^2) = 0 \in \mathbb{R}^{2N}, \quad w = [u_1, \dots, u_N, v_1 \dots v_N]^\top \in \mathbb{R}^N \times \mathbb{R}^N = \mathbb{R}^{2N}. \tag{2.16}$$

There exists the arc length parameterization of (2.16),

$$F(w(s), L^2(s)) = 0 \in \mathbb{R}^{2N}, \quad w(s) = [u_1(s), \dots, u_N(s), v_1(s), \dots, v_N(s)]^\top \in \mathbb{R}^{2N},$$

$s \in \mathbb{R}^1$, see, e.g., [1], p. 14. We can define the positive/negative orientation of this curve.

We consider numerical continuation methods (i.e., tracing of implicitly defined curves) using predictor-corrector methods, see, e.g., [1], [5]. We refer to the ready-made continuation software in matcont_manual [6]: see Section 7, Equilibrium continuation, generic bifurcation of codim 1. These bifurcation points are a) limit point (fold), LP, b) Hopf point, H, c) branching point, BP. For the classification of these bifurcation points see also [15].

We need to specify the kinetics of model (2.8). We consider the Schnakenberg model [18] and the corresponding discretization

$$\begin{aligned} \mathbf{u}_t &= \frac{d_1}{L^2}\mathbf{u}_{xx} + \gamma(a - \mathbf{u} + \mathbf{u}^2\mathbf{v}), \\ \mathbf{v}_t &= \frac{d_2}{L^2}\mathbf{v}_{xx} + \gamma(b - \mathbf{u}^2\mathbf{v}) \end{aligned} \tag{2.17}$$

in the domain $0 \leqslant x \leqslant 1$ with no flux boundary condition

$$\mathbf{u}_x(0,t) = \mathbf{u}_x(1,t) = 0, \quad \mathbf{v}_x(0,t) = \mathbf{v}_x(1,t) = 0.$$

The parameters of the model are $a > 0$, $b > 0$, $\gamma > 0$. The model has a homogeneous steady state

$$\mathbf{u} = a + b, \quad \mathbf{v} = \frac{b}{(a+b)^2}. \tag{2.18}$$

The aim is to find the discrete steady states (2.8) with respect to specific kinetics (2.17). The resulting system reads as follows

(2.19)

$$
\begin{aligned}
F_1(w, L^2) &\equiv 2\frac{d_1}{h^2L^2}(-u_1 + u_2) + \gamma(a - u_1 + u_1^2 v_1) = 0,\\
F_i(w, L^2) &\equiv \frac{d_1}{h^2L^2}(u_{i-1} - 2u_i + u_{i+1}) + \gamma(a - u_i + u_i^2 v_i) = 0, \quad i = 2, \ldots, N-1,\\
F_N(w, L^2) &\equiv 2\frac{d_1}{h^2L^2}(u_{N-1} - u_N) + \gamma(a - u_N + u_N^2 v_N) = 0,\\
F_{N+1}(w, L^2) &\equiv 2\frac{d_2}{h^2L^2}(-v_1 + v_2) + \gamma(b - u_1^2 v_1) = 0,\\
F_{N+i}(w, L^2) &\equiv \frac{d_2}{h^2L^2}(v_{i-1} - 2v_i + v_{i+1}) + \gamma(b - u_i^2 v_i) = 0, \quad i = 2, \ldots, N-1,\\
F_{2N}(w, L^2) &\equiv 2\frac{d_2}{h^2L^2}(v_{N-1} - v_N) + \gamma(b - u_N^2 v_N) = 0.
\end{aligned}
$$

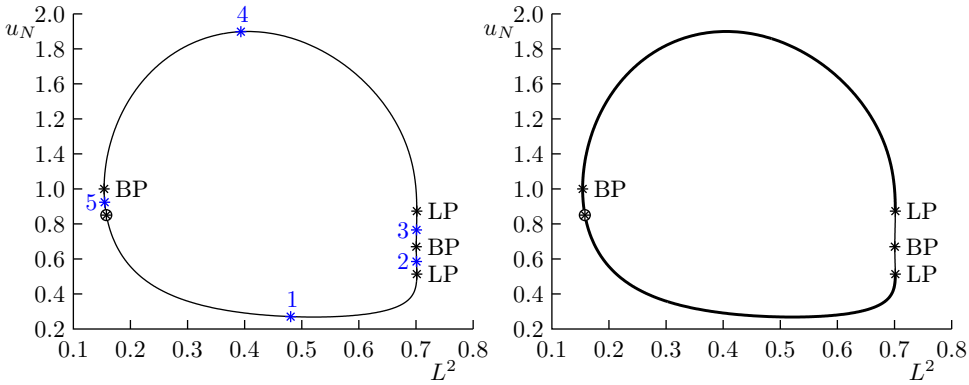

Figure 1. Left: Branch of inhomogeneous steady states projected onto pairs (u_N, L^2). The circle on the branch indicates the starting point of the continuation procedure. Stability is tested at points $1, \ldots, 5$. Right: thick and thin curve segments indicate stable and unstable steady states.

E x a m p l e 2.1. Consider the system (2.19) for the parameter settings $a = 0.1$, $b = 0.9$, $\gamma = 10$, $d_1 = 0.1$, $d_2 = 1.6$ and $N = 20$. The coordinates $w^* \in \mathbb{R}^{2N}$ of the homogeneous state (2.9) can be calculated as $u^* = a+b = 1$ and $v^* = b/(a+b)^2 = 0.9$, see (2.18).

The aim is to compute a branch of inhomogeneous steady states (2.16) emanating from a particular primary bifurcation point.

The primary bifurcation points $(w^*, (L^*)^2)$ are sorted in ascending order. The primary bifurcation point $(w^*, (L^*)^2)$ with the smallest value of positive $(L^*)^2 > 0$ is $(L^*)^2 \approx 0.1539$. We can compute this point in double precision.

Figure 1 shows a branch (2.16) projected onto the pairs (u_N, L^2). The closed curve on the left is computed using continuation software, see matcont_manual [6]: Section 7, Equilibrium continuation. However, the branch needs to be initialized, which is not straightforward: To determine the *initial point* of the branch we use the formula (2.15) with $\delta = 0.1$ as predictor.

The branch is oriented counterclockwise. The continuation software calculates bifurcation points, which are (counterclockwise) LP, BP, LP and BP. It is obvious that the primary bifurcation point BP is caused by the crossing of the homogeneous steady states (2.9) with inhomogeneous steady states (2.16), whereas the *secondary bifurcation point* BP is not related to such a crossing. Both the primary and secondary ones are called *branching points*. The continuation software identifies branch points BP. The distinction (primary/secondary) depends on the context. Branching points BP are further classified in Section 4 as symmetry-breaking bifurcation points.

The branch (2.16) consists of segments $1, \ldots, 5$. In each segment, there is a test-point on the curve and Jacobian is calculated. If the largest real part of the relevant eigenvalues is negative, the test-point is declared stable and the whole segment is declared stable. We do not compute all the eigenvalues of the Jacobian. We use the Matlab function `d = eigs` $('Jacobian', 6, 'lr')$, which computes the six "right-most" eigenvalues. The stability condition is therefore `real(d) < 0`. We also comment on the choice of test-points on the curve. We calculate the arclength of each specific segment numerically. The test point shall be positioned so that the arc length is halved.

R e m a r k 2.1. The continuation algorithm [6] defines the projection of branches onto pairs (u_i, L^2) and (v_i, L^2), respectively, for each $i = 1, \ldots, N$. Consider the projection (u_N, L^2) as a reference. It serves for a kind of "dimensional reduction".

R e m a r k 2.2 (Algorithm of continuation: novelties).
(a) initialization of the branch via (2.15),
(b) branch segmentation, distinguishing stable and unstable branch segments.

In following Section 3 we obtain the formulae for all primary bifurcation points.

3. Dispersion equation

We consider the system (2.2). Let $u^* \in \mathbb{R}^1$, $v^* \in \mathbb{R}^1$ be a homogeneous steady state, i.e.,

$$f(u^*, v^*) = g(u^*, v^*) = 0, \quad 0 \leqslant x \leqslant 1.$$

In particular,

$$u^* = a + b, \quad v^* = \frac{b}{(a+b)^2}, \quad a > 0,\ b > 0, \tag{3.1}$$

is the steady state calculated by the Schnakenberg model.

In general, we define the Jacobian at the steady state $u^* \in \mathbb{R}^1$, $v^* \in \mathbb{R}^1$:

$$\mathbf{J} = \begin{bmatrix} f_u & f_v \\ g_u & g_v \end{bmatrix}_{u,v:=u^*,v^*}. \tag{3.2}$$

In particular,

$$\mathbf{J} = \begin{bmatrix} 2\gamma b/(a+b) - 1 & (a+b)^2 \\ -2b/(a+b) & -(a+b)^2 \end{bmatrix}, \quad a > 0,\ b > 0,\ \gamma > 0, \tag{3.3}$$

for the Schnakenberg model.

Recall (2.2). Let d_1 and d_2 be diffusion parameters. Let $\mathbf{J}$ be the Jacobian (3.2) corresponding to the steady state. The equation

$$\det\left(\mathbf{J} - k^2 \begin{bmatrix} d_1 & 0 \\ 0 & d_1 \end{bmatrix} - \lambda \mathbf{I}\right) = 0, \quad \mathbf{I} = \mathbf{I}_{2\times 2} \in \mathbb{R}^{2\times 2}, \tag{3.4}$$

is called the *dispersion relation*, see, e.g., [17] p. 382. It depends on the *wavenumber* k^2 and *frequency* λ. The dispersion relation (3.4) implicitly defines the relation $\lambda = \lambda(k^2)$.

Instead of analyzing the roots of the dispersion relation (3.4), we analyze the spectrum of the matrix

$$\mathbf{H} = \mathbf{J} - k^2 \begin{bmatrix} d_1 & 0 \\ 0 & d_1 \end{bmatrix}. \tag{3.5}$$

The spectrum $\sigma(\mathbf{H})$ consists of two eigenvalues $\{\lambda_1(k^2), \lambda_2(k^2)\}$. These can be numerically computed as a function of k^2. We use the Matlab function `eig(H)`. Note that in general $\sigma(\mathbf{H})$ consists of either two real eigenvalues or a complex conjugate pair.

For a given k^2, we put

$$\Re(\lambda_*(k^2)) = \max\{\Re(\lambda_i(k^2))\}_{i=1,2}, \tag{3.6}$$

which is the right-most eigenvalue of $\sigma(\mathbf{H})$. We call $\Re(\lambda_*(k^2))$ the *maximal growth rate*. When the value of k^2 is chosen, the next Matlab script

```
≫ H = J - k^2*[d_1 0;0 d_2];
≫ [VV,DD] = eig(H);
≫ [right_most,i_max] = max(real(diag(DD)));
```

returns the value `right_most` $= \Re(\lambda_*(k^2))$. Figure 2 shows scan of the function $\Re(\lambda_*(k^2))$ related to Example 2.1.

Consider the roots of the function $k^2 \mapsto \Re(\lambda_*(k^2))$. They are marked with two dots in Figure 2. In general, there are two roots, if any. It corresponds to the fact that the dispersion equation (3.4) is a quadratic equation.

Let k_-^2 and k_+^2, $k_-^2 \leqslant k_+^2$, be the roots of the function $k^2 \mapsto \Re(\lambda_*(k^2))$. We can get closed-form expressions

$$k_-^2 = \frac{d_2 f_u + d_1 g_v - \sqrt{\Delta}}{2 d_1 d_2}, \quad k_+^2 = \frac{d_2 f_u + d_1 g_v + \sqrt{\Delta}}{2 d_1 d_2}, \tag{3.7}$$

where $\Delta = (d_2 f_u + d_1 g_v)^2 - 4 d_1 d_2 \det \mathbf{J}$, and $\mathbf{J}$, f_u, g_v are related to the Jacobian (3.2).

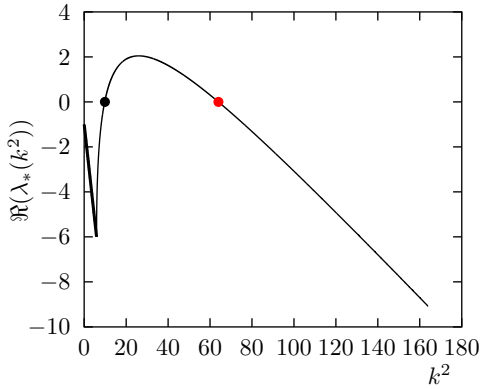

Figure 2. Schnakenberg model, Example 2.1. The maximal growth rate $k^2 \mapsto \Re(\lambda_*(k^2))$: the thin and thick curve segments refer to two real eigenvalues and complex conjugate pairs, respectively.

The open interval (k_-^2, k_+^2) is called the *range of growing wave numbers*. For a given k^2, $k_-^2 < k^2 < k_+^2$, the maximal growth rate is positive.

Definition 3.1. Consider the formula (3.7). If $k_-^2 = k_+^2$, we say that the relevant wavenumber is critical. Let us call it k_c.

The aim is to analyze the spatial pattern formation by linear stability analysis. We follow [17], 14.3. We consider the system (2.2) linearized about a homogeneous steady state $u^* \in \mathbb{R}^1$, $v^* \in \mathbb{R}^1$, with the appropriate boundary conditions (2.3)

$$\begin{bmatrix} \mathbf{u}_t \\ \mathbf{v}_t \end{bmatrix} = \mathbf{J} \begin{bmatrix} \mathbf{u} \\ \mathbf{v} \end{bmatrix} + \frac{1}{L^2} \begin{bmatrix} d_1 & 0 \\ 0 & d_1 \end{bmatrix} \begin{bmatrix} \mathbf{u}_{xx} \\ \mathbf{v}_{xx} \end{bmatrix} \tag{3.8}$$

in the range $0 \leqslant x \leqslant 1$. We apply the Fourier analysis by setting

$$\begin{bmatrix} \mathbf{u}(x,t) \\ \mathbf{v}(x,t) \end{bmatrix} = \sum_{j=1}^{\infty} \mathbf{c}_j \mathrm{e}^{\lambda t} W_j(x), \quad 0 \leqslant x \leqslant 1,\ t \geqslant 0, \tag{3.9}$$

where $\mathbf{c}_j \in \mathbb{R}^2$ are the coefficients to be determined, $\lambda \in \mathbb{R}^1$ defines the temporal growth. The Fourier functions W_j are related to the 1-D Laplacian with the Neumann boundary conditions

$$W_j'' + k^2 W_j = 0, \quad 0 \leqslant x \leqslant 1, \quad W_j'(0) = W_j'(1) = 0. \tag{3.10}$$

The relevant eigenvalues are $k^2 = (j\pi)^2$, while the corresponding eigenvectors are $W_j = \sqrt{2}\cos(j\pi x)$ for $j = 1, 2, \ldots$

Substituting (3.9) into (3.8) with (3.10), and canceling $\mathrm{e}^{\lambda t}$, we conclude that

$$\det\left(\mathbf{J} - \frac{k^2}{L^2}\begin{bmatrix} d_1 & 0 \\ 0 & d_1 \end{bmatrix} - \lambda \mathbf{I}\right) = 0, \quad \mathbf{I} = \mathbf{I}_{2\times 2} \in \mathbb{R}^{2\times 2}. \tag{3.11}$$

The equation (3.11) is analogous to the dispersion relation (3.4). It depends on the frequency λ, a particular eigenvalue $k^2 = (j\pi)^2$, $j = 1, 2, \ldots$, and the wavelength L^2. The roots of (3.11) are related to the spectrum of the matrix $\mathbf{H}$,

$$\mathbf{H} = \mathbf{J} - \frac{k^2}{L^2}\begin{bmatrix} d_1 & 0 \\ 0 & d_1 \end{bmatrix}. \tag{3.12}$$

Its spectrum consists of two eigenvalues $\{\lambda_1(k^2/L^2), \lambda_2(k^2/L^2)\}$. Similarly to (3.6) we define the maximal growth rate as a function

$$\frac{k^2}{L^2} \mapsto \Re\Big(\lambda_*\Big(\frac{k^2}{L^2}\Big)\Big) \equiv \max\Big\{\Re\Big(\lambda_i\Big(\frac{k^2}{L^2}\Big)\Big)\Big\}_{i=1,2}. \tag{3.13}$$

We ask for k^2/L^2 when $\Re(\lambda_*(k^2/L^2))$ is positive. Consider the case of the transition $\Re(\lambda_*(k^2/L^2)) = 0$. So we are looking for the roots of the above function. We observe that the roots are given by the formula (3.7). For the parameters k^2 and L^2 that satisfy $k_-^2 < k^2/L^2 < k_+^2$ we can expect the existence of an inhomogeneous steady state. As for the wavelength L^2, we have reached the restriction

$$\frac{k^2}{k_+^2} < L^2 < \frac{k^2}{k_-^2}. \tag{3.14}$$

The estimate (3.14) of the stable wavelength range is related to the partial differential equation (3.8). The state variables are the functions $\mathbf{u}(x,t)$ and $\mathbf{v}(x,t)$, see (3.9). We decided to discretize the state variables for numerical purposes.

For this purpose, we consider the spectrum of a discrete 1-D Laplacian with Neumann boundary conditions on the equidistant grid (2.4). For relevant formulas, see Remark 3.1.

In particular, we define the function $[e\_val, e\_vec] = Lap\_neum(N, No)$ where N is the number of mesh points and No is the serial number of the eigenmode. The function Lap_neum returns the corresponding eigenvalue $e\_val \in \mathbb{R}^1$ and the eigenvector $e\_vec \in \mathbb{R}^N$. By definition: If $No = 0$ then $e\_val = 0$. The positive eigenvalues are ordered: $No = 1, \ldots, N-1$ from the smallest to the largest one.

R e m a r k 3.1. Spectrum of a discrete 1-D Laplacian with Neumann boundary conditions on the equidistant grid (2.4):

$[e\_val, e\_vec] = Lap\_neum(N, No)$,
$e\_val = 2/h^2[1 - \cos(j\pi/N)]$, $No = j = 1, \ldots, N-1$, $h = 1/(N+1)$,
$e\_vec \in \mathbb{R}^N$, the sampled eigenfunction of W_j, see (3.10).

Using the above notation, we formulate suitable discrete analogies of (3.11)–(3.14). In particular, we set

$$k^2 = e\_val = Lap\_neum(N, No), \quad No = j \in \{1, \ldots, N-1\}. \tag{3.15}$$

To simplify the notation, e_val and e_vec are generic value variables, and $No = j \in \{1, \ldots, N-1\}$.

We define the function

$$L^2 \mapsto \Re(\lambda_*(L^2, No = j)) \equiv \max\Big\{\Re\Big(\lambda_i\Big(\frac{e\_val}{L^2}\Big)\Big)\Big\}_{i=1,2}, \tag{3.16}$$

$j \in \{1, \ldots, N-1\}$. We call it the *maximal growth rate*. We can scan it using a similar algorithm as for the function (3.6).

Definition 3.2. Given the mode number $No = j \in \{1, \ldots, N-1\}$, we introduce the interval

$$\frac{e\_val}{k_+^2} < L^2 < \frac{e\_val}{k_-^2} \tag{3.17}$$

and call it the *stable wavelength range*. We define

$$L2\_No\_up = \frac{e\_val}{k_+^2}, \quad L2\_No\_down = \frac{e\_val}{k_-^2} \tag{3.18}$$

as the *critical wavelengths* related to the mode number $No = j \in \{1, \ldots, N-1\}$.

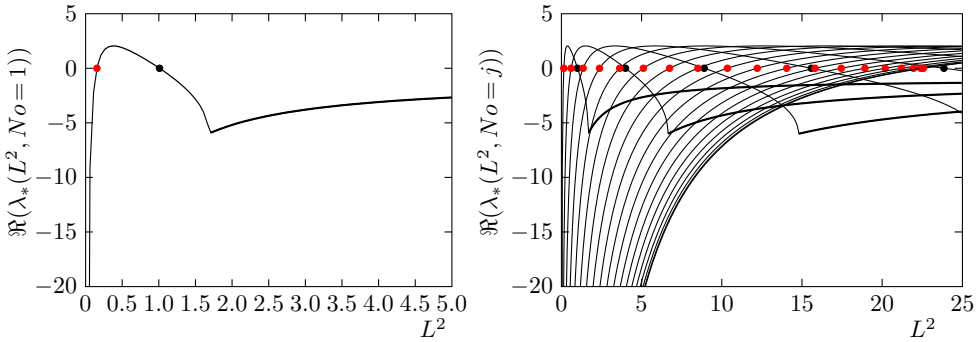

Figure 3. Schnakenberg model, Example 2.1: Left: The first stable wavelength range, $L2\_1\_up < L^2 < L2\_1\_down$, $L2\_1\_up \approx 0.1542$, $L2\_1\_down \approx 1.0098$. Right: Critical wavelengths for $j \in \{1, \ldots, N-1\}$. Higher stable wavelength ranges $L2\_j\_up < L^2 < L2\_j\_down$.

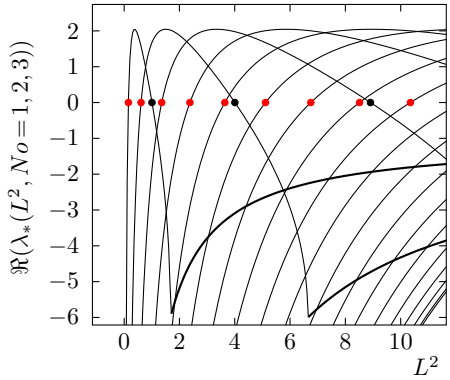

Figure 4. Schnakenberg model, Example 2.1. Critical wavelengths for $j \in \{1, \ldots, N-1\}$, sorted in ascending order: $L2\_1\_up$, $L2\_2\_up$, $L2\_1\_down$, $L2\_3\_up$, $L2\_4\_up$, $L2\_5\_up$, $L2\_2\_down$, $L2\_6\_up$, etc.

An example of critical wavelengths is shown in Figure 3 on the left: $L2\_1\_up$ is the smallest critical point available. In the stable wavelength range $L2\_1\_up < L^2 < L2\_1\_down$ we can expect the existence of an inhomogeneous steady state due to the linearized stability argument. We consider *all* critical wavelengths for $j \in \{1, \ldots, N-1\}$, see Figure 3 right. For a zoom, see Figure 4. The first eight critical wavelengths are listed in Table 1.

Crit. wave	1	2	3	4	5	6	7	8
Label	$L2\_1\_up$	$L2\_2\_up$	$L2\_1\_down$	$L2\_3\_up$	$L2\_4\_up$	$L2\_5\_up$	$L2\_2\_down$	$L2\_6\_up$
Value $\approx$	0.1539	0.6114	1.0081	1.3601	2.3794	3.6417	4.0047	5.1125
Mode	1	2	1	3	4	5	2	6

Table 1. Schnakenberg model, Example 2.1: Sorted critical wavelengths.

Recall that *e_val* and *e_vec* are generic value variables. We put

$$\xi \equiv \begin{bmatrix} a \\ b \end{bmatrix} \otimes e\_vec \in \mathbb{R}^{2N}, \tag{3.19}$$

where $\otimes$ is the Kronecker product of the two matrices above. In the standard Matlab notation, $\xi = [a .^* e\_vec; b .^* e\_vec]$, where the operator $.^*$ is the element-wise multiplication.

There is a correlation between the critical wavelengths and the primary bifurcation points. Let $a_{up} \in \mathbb{R}^1$, $b_{up} \in \mathbb{R}^1$, and $a_{down} \in \mathbb{R}^1$, $b_{down} \in \mathbb{R}^1$ be the solutions of linear systems

$$\left(\mathbf{J} - k_+^2 \begin{bmatrix} d_1 & 0 \\ 0 & d_1 \end{bmatrix}\right) \begin{bmatrix} a_{up} \\ b_{up} \end{bmatrix} = 0, \ \left(\mathbf{J} - k_-^2 \begin{bmatrix} d_1 & 0 \\ 0 & d_1 \end{bmatrix}\right) \begin{bmatrix} a_{down} \\ b_{down} \end{bmatrix} = 0, \tag{3.20}$$

respectively, where k_+^2 and k_-^2 are defined in (3.7). Let

$$\xi_{up} \equiv \begin{bmatrix} a_{up} \\ b_{up} \end{bmatrix} \otimes e\_vec \in \mathbb{R}^{2N}, \quad \xi_{down} \equiv \begin{bmatrix} a_{down} \\ b_{down} \end{bmatrix} \otimes e\_vec \in \mathbb{R}^{2N}. \tag{3.21}$$

Theorem 3.1. *For a given $j \in \{1, \ldots, N-1\}$, let L2_j_up and L2_j_down be the critical wavelengths. Let $\xi_{up} \in \mathbb{R}^{2N}$ and $\xi_{down} \in \mathbb{R}^{2N}$ be defined as in* (3.21). *Then L2_j_up and L2_j_down are related to the primary bifurcation points $F(w^*, L2\_j\_up) = 0 \in \mathbb{R}^N$, $F_w(w^*, L2\_j\_up)\xi_{up} = 0 \in \mathbb{R}^{2N}$, and $F(w^*, L2\_j\_down) = 0 \in \mathbb{R}^N$, $F_w(w^*, L2\_j\_down)\xi_{down} = 0 \in \mathbb{R}^{2N}$.*

P r o o f. Consider *L2_j_up*. By (3.18), $L2\_No\_up = e\_val/k_+^2$. Recall (3.12). In this context

$$\mathbf{H} = \mathbf{J} - \frac{e\_val}{L2\_j\_up} \begin{bmatrix} d_1 & 0 \\ 0 & d_1 \end{bmatrix} = \mathbf{J} - k_+^2 \begin{bmatrix} d_1 & 0 \\ 0 & d_1 \end{bmatrix}. \tag{3.22}$$

We investigate the spectrum of the matrix $\mathbf{H}$:

```
≫ [VV,DD] = eig(H);
≫ [right_most,i_max] = max(real(diag(DD)));
```

The right-most eigenvalue is equal to zero. Therefore,

$$\gg \texttt{DD} = \begin{bmatrix} 0 & 0 \\ 0 & r \end{bmatrix}, \ r < 0.$$

Let `VV(:,1)` be the first column of the matrix `VV`. We denote this column as $\begin{bmatrix} a \\ b \end{bmatrix}$. We conclude that

$$\left(\mathbf{J} - k_+^2 \begin{bmatrix} d_1 & 0 \\ 0 & d_1 \end{bmatrix}\right) \begin{bmatrix} a \\ b \end{bmatrix} = 0 \in \mathbb{R}^2$$

and

$$\left(\mathbf{J} - k_+^2 \begin{bmatrix} d_1 & 0 \\ 0 & d_1 \end{bmatrix}\right) \begin{bmatrix} a \\ b \end{bmatrix} \otimes e\_vec = 0 \in \mathbb{R}^{2N}.$$

Therefore,

$$F_w(w^*, L2\_j\_up) \begin{bmatrix} a \\ b \end{bmatrix} \otimes e\_vec = \left(\mathbf{J} - k_+^2 \begin{bmatrix} d_1 & 0 \\ 0 & d_1 \end{bmatrix}\right) \begin{bmatrix} a \\ b \end{bmatrix} \otimes e\_vec = 0 \in \mathbb{R}^{2N}.$$

Note that $a = a_{up}$, $b = b_{up}$, see (3.20). Hence, for ξ_{up}, see (3.21).

Let $L2\_j\_down$ be the critical wavelength. We can mimic the above arguments to show that $L2\_j\_down$ is related to the primary bifurcation point. □

R e m a r k 3.2. Based on Theorem 3.1, we can identify the critical wavelength with the primary bifurcation point. Primary bifurcation points appear in pairs. We can calculate and sort all $2(N-1)$ bifurcation points.

R e m a r k 3.3. Now we can finally classify the primary bifurcation points, which appear in Figure 1 as $(L^\star)^2 = L2\_1\_up \approx 0.1539$.

Consider a branch of homogeneous steady states parameterized by L^2, see formulae (2.9). Given L^2, let $F_w(w^*, L^2) \in \mathbb{R}^{2N \times 2N}$ be the Jacobian at the point $(w^*, L^2) \in \mathbb{R}^{2N} \times \mathbb{R}^1$. We recall the classification of steady states [15], p. 42: Let n_-, n_0, and n_+ be the number of eigenvalues of the matrix $F_w(w^*, L^2)$ (counting multiplicities) with negative, zero, and positive real part, respectively. We say that the triple $[n_-, n_0, n_+]$ is the signature of the steady state $(w^*, L^2) \in \mathbb{R}^{2N} \times \mathbb{R}^1$.

$0 \leqslant L^2 < L2\_1\_up$	[40,0,0]	$L2\_1\_up$	[39,1,0]
$L2\_1\_up < L^2 < L2\_2\_up$	[39,0,1]	$L2\_2\_up$	[38,1,1]
$L2\_2\_up < L^2 < L2\_1\_down$	[38,0,2]	$L2\_1\_down$	[38,1,1]
$L2\_1\_down < L^2 < L2\_3\_up$	[38,0,2]	$L2\_3\_up$	[38,1,1]
$L2\_3\_up < L^2 < L2\_4\_up$	[38,0,2]	$L2\_4\_up$	[37,1,2]
$L2\_4\_up < L^2 < L2\_5\_up$	[37,0,3]	$L2\_5\_up$	[36,1,3]
$L2\_5\_up < L^2 < L2\_2\_down$	[36,0,4]	$L2\_2\_down$	[36,1,3]
$L2\_2\_down < L^2 < L2\_6\_up$	[36,0,4]	$L2\_6\_up$	[36,1,3]

Table 2.

In the context of the Schnakenberg model, see Example 2.1, we consider the branch of homogeneous steady states parameterized by L^2 that span the interval $[0, L2\_6\_up]$, $L2\_6\_up \approx 5.1125$. The classification is summarized in Table 2. Note that we do not need to compute the full spectrum for the current value of the parameter L^2 to obtain the signature $[n_-, n_0, n_+]$. Just recall that the signature varies incrementally at the bifurcation points.

4. Symmetries of the state space

Consider the abstract group $\Gamma = \mathbb{Z}_2 \oplus \mathbb{Z}_2 = \{\iota, \kappa_1, \kappa_2, \kappa_1\kappa_2\}$, $\kappa_1\kappa_2 = \kappa_2\kappa_1$. Here $\mathbb{Z}_2$ is a cyclic group of order 2 and $\mathbb{Z}_2 \oplus \mathbb{Z}_2$ is a direct sum of groups. Therefore, Γ is an Abelian group.

We consider the following matrices: the *identity matrix*, the *zero matrix* and the *exchange matrix* of the proper size:

$$\mathbf{I}_{2N\times 2N} \in \mathbb{R}^{2N\times 2N}, \quad \mathbf{O}_{N\times N} \in \mathbb{R}^{N\times N}, \quad \mathbf{E} = \begin{bmatrix} 0 & & 1 \\ & \iddots & \\ 1 & & 0 \end{bmatrix} \in \mathbb{R}^{N\times N}. \tag{4.1}$$

We define the matrix representation of the group Γ in the state space $\mathbb{R}^{2N}$ as

$$\mathbf{G}(\iota) = \mathbf{I}_{2N\times 2N} \in \mathbb{R}^{2N\times 2N}, \quad \mathbf{G}(\kappa_1) = -\mathbf{I}_{2N\times 2N} \in \mathbb{R}^{2N\times 2N}, \tag{4.2}$$

$$\mathbf{G}(\kappa_2) = \begin{bmatrix} \mathbf{E} & \mathbf{O}_{N\times N} \\ \mathbf{O}_{N\times N} & \mathbf{E} \end{bmatrix} \in \mathbb{R}^{2N\times 2N}, \tag{4.3}$$

$$\mathbf{G}(\kappa_1\kappa_2) = \mathbf{G}(\kappa_1)\mathbf{G}(\kappa_2) = -\mathbf{G}(\kappa_2) = \mathbf{G}(\kappa_2\kappa_1). \tag{4.4}$$

We resume, that $\Gamma = \{\mathbf{G}(\iota), \mathbf{G}(\kappa_1), \mathbf{G}(\kappa_2), \mathbf{G}(\kappa_1\kappa_2)\}$ is an Abelian group with faithful representation in the state space $\mathbb{R}^{2N}$. Each element of the group $\gamma \in \Gamma$ is identified by its action, namely by a linear transformation $\mathbb{R}^{2N\times 2N}$. To simplify the notation, we identify the mentioned linear transformations with elements of the group $\Gamma = \{\iota, \kappa_1, \kappa_2, \kappa_1\kappa_2\}$.

The group Γ has proper subgroups $\Sigma_{\kappa_1} = \{\iota, \kappa_1\}$, $\Sigma_{\kappa_2} = \{\iota, \kappa_2\}$, $\Sigma_{\kappa_1\kappa_2} = \{\iota, \kappa_1\kappa_2\}$ and $\Sigma_0 = \{\iota\}$. We must recall two notions of representation theory: the *isotropy subgroup* Σ, see [9], (1.2), p. 69, and the *fixed-point subspace* $\operatorname{Fix}\Sigma$ *of a subgroup* Σ, see [9], (2.1), p. 74. We have

$$\begin{aligned} \operatorname{Fix}_{\mathbb{R}^{2N}} \Sigma_{\kappa_1} &= \operatorname{Fix}_{\mathbb{R}^{2N}} \Gamma = 0 \in \mathbb{R}^{2N}, \\ \operatorname{Fix}_{\mathbb{R}^{2N}} \Sigma_{\kappa_2} &= \{w \in \mathbb{R}^{2N} \colon\ w_i = w_{N-i+1},\ w_{N+i} = w_{2N-i+1},\ i = 1, \dots, N\}, \\ \operatorname{Fix}_{\mathbb{R}^{2N}} \Sigma_{\kappa_1\kappa_2} &= \{w \in \mathbb{R}^{2N} \colon\ w_i = -w_{N-i+1},\ w_{N+i} = -w_{2N-i+1},\ i = 1, \dots, N\}, \\ \operatorname{Fix}_{\mathbb{R}^{2N}} \Sigma_0 &= \mathbb{R}^{2N}. \end{aligned} \tag{4.5}$$

Here Σ_{κ_2}, $\Sigma_{\kappa_1\kappa_2}$ and Σ_0 are isotropy subgroups of Γ. Moreover, Σ_{κ_2} and $\Sigma_{\kappa_1\kappa_2}$ are *maximal isotropy subgroups*, see [9], Definition 2.6, p. 78.

We recall the manifold of the steady state solutions (2.8). By specifying the kinetics, we define a discrete version of the Schnakenberg model (2.19). A key feature of this model is the Γ-*equivariance*:

$$F(\gamma w, L^2) = \gamma F(w, L^2) \tag{4.6}$$

for $(w, L^2) \in \mathbb{R}^{2N} \times \mathbb{R}^1$, for all $\gamma \in \{\iota, \kappa_1, \kappa_2, \kappa_1\kappa_2\}$. Property (4.6) can be immediately verified. We speak of the equivariant theory of bifurcations, see, e.g., [4].

Consider the Schnakenberg model, Example 2.1, assuming $N = 40$. Figure 5 shows branches of inhomogeneous steady states emanating from the primary bifurcation points *L2_3_up* (on the left) and *L2_4_up* (on the right). Projection onto the pairs (u_N, L^2) is applied. The thick and thin segments of the curves indicate stable and unstable steady states. We place random test points $*$ on the stable segments.

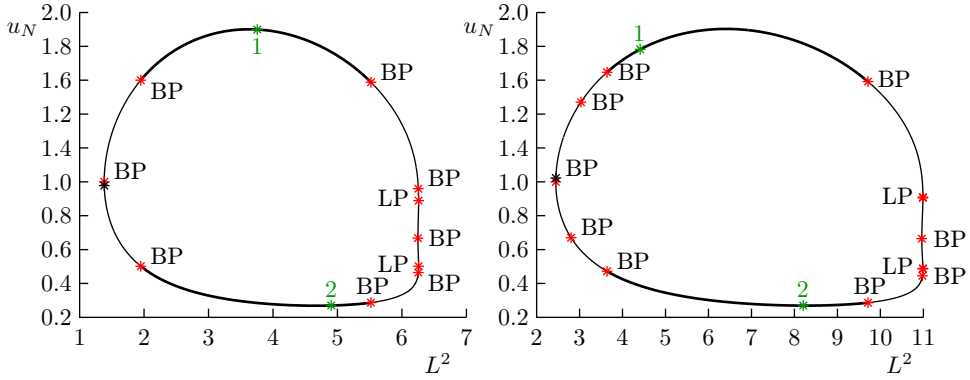

Figure 5. Schnakenberg model, Example 2.1, $N = 40$. Branches of inhomogeneous steady states projected onto pairs (u_N, L^2), emanating from *L2_3_up* (left) and *L2_4_up* (right). Thick and thin segments of the curves denote the stable and unstable steady state segments, respectively. The random test points $*$ are placed on the stable segments.

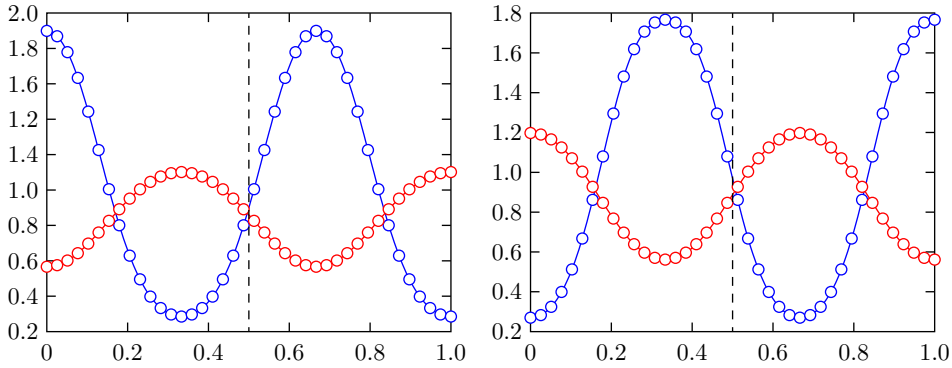

Figure 6. Schnakenberg model, Example 2.1, $N = 40$, the branch *L2_3_up*: Consider the steady states $[u_1, \dots, u_N, v_1, \dots, v_N]^\top \in \mathbb{R}^{2N}$ related to the two marked test points $*$ in Figure 5 left. Both the steady states $[u_1, \dots, u_N]^\top$ (blue) and $[v_1, \dots, v_N]^\top$ (red) are antisymmetric functions with respect to the center line $x = \frac{1}{2}$.

Our aim is to investigate the *symmetry* of the steady state branches of (2.16). We visualize them on particular examples. In general, the symmetries will occur in the maximal one of isotropy subgroups $\Sigma_{\kappa_1\kappa_2}$ and Σ_{κ_2}. We show the steady states $[u_1, \dots, u_N]^\top \in \mathbb{R}^N$ and $[v_1, \dots, v_N]^\top \in \mathbb{R}^N$, which are

▷ discrete *antisymmetric* functions, in the first case,

▷ discrete *symmetric* functions, in the second case.

Figure 6 shows steady states related to the test points 1 and 2 on the stable segments, see Figure 5 left. Plots of the steady states $[u_1, \dots, u_N]^\top$ (blue) and $[v_1, \dots, v_N]^\top$ (red) are antisymmetric functions with respect to the center line $x = \frac{1}{2}$.

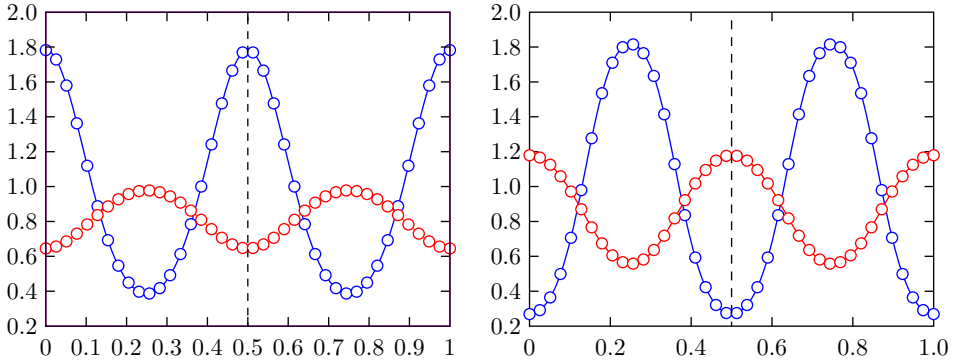

Figure 7. Schnakenberg model, Example 2.1, $N = 40$, the branch *L2_4_up*: Consider the steady states $[u_1, \dots, u_N, v_1, \dots, v_N]^\top \in \mathbb{R}^{2N}$ related to the two marked test points $*$ in Figure 5 right. Both the steady states $[u_1, \dots, u_N]$ (blue) and $[v_1, \dots, v_N]$ (red) are symmetric functions with respect to the center line $x = \frac{1}{2}$.

Figure 7 shows the steady states related to the test points 1 and 2 on the stable segments, see Figure 5 right. Graphs of the steady states $[u_1, \dots, u_N]^\top$ (blue) and $[v_1, \dots, v_N]^\top$ (red) are symmetric functions with respect to the center line $x = \frac{1}{2}$.

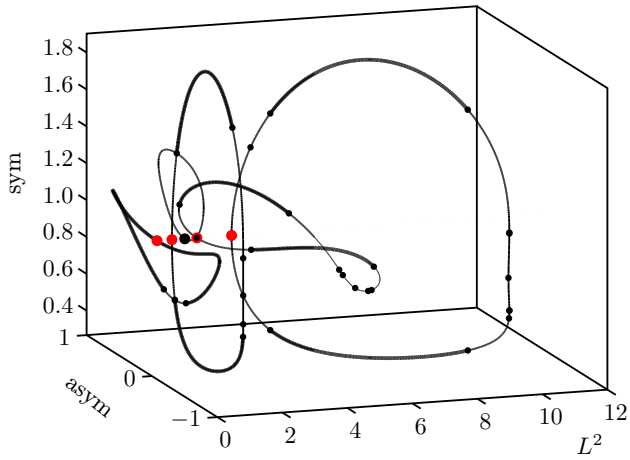

Figure 8. Schnakenberg model, Example 2.1, $N = 40$. Homogeneous steady states are not displayed. The branches of inhomogeneous steady states emanating from *L2_1_up*, *L2_2_up*, *L2_1_down*, *L2_3_up*, *L2_4_up*.

We use a 3-pair projector to visualize branches of the inhomogeneous steady states

$$\texttt{sym} \equiv \frac{u_1 + u_N}{2}, \quad \texttt{asym} \equiv \frac{u_1 - u_N}{2}, \quad L^2. \tag{4.7}$$

The projector (4.7) is called a *symmetry-adapted filter*. The filter is invariant with respect to each fixed-point subspace of (4.5). Figure 8 shows the global bifurcation diagram using the symmetry-adapted filter. The diagram includes the first five branches emanating from the bifurcation points *L2_1_up*, *L2_2_up*, *L2_1_down*, *L2_3_up*, *L2_4_up*.

5. Continuation versus dynamic simulation

Consider numerical procedures for calculating inhomogeneous steady states. In addition to numerical continuation, we discuss a technique called dynamic simulation. The latter is currently in use. We recall it in the following remark.

Remark 5.1 (Dynamic simulation). Consider the operator (2.6). Instead of seeking for the steady states (i.e. the roots of the nonlinear system (2.8)) we define the initial value problem

$$t \in \mathbb{R}^1 \mapsto w(t) = [u_1(t), \ldots, u_N(t), v_1(t), \ldots, v_N(t)]^\top \in \mathbb{R}^{2N}, \tag{5.1}$$

L is fixed. The initial condition $w^0 \in \mathbb{R}^{2N}$ is usually considered to be the randomly perturbed homogeneous steady state (2.9). It is expected that $w(t) \in \mathbb{R}^{2N} \mapsto [u_1, \ldots, u_N, v_1, \ldots, v_N]^\top \in \mathbb{R}^{2N}$ as $t \in \mathbb{R}^1 \mapsto \infty$. Thus, in the case of convergence, the vector $[u_1, \ldots, u_N, v_1, \ldots, v_N]^\top$ can be an *inhomogeneous* steady state related to some parameter L. Let us call the above procedure the *dynamic simulation*.

We are going to illustrate that

(1) dynamic simulations can converge to steady states that are not unique,
(2) they may not converge at all.

We consider the first stable wavelength range, $L2\_1\_up < L^2 < L2\_1\_down$, $L2\_1\_up \approx 0.1542$, $L2\_1\_down \approx 1.0098$, see Figure 3.

For comparison, consider the branch *L2_1_up*, see Figure 1. We place five test points on the branch. At a particular test point, we perform a dynamic simulation with the fixed ordinate L^2. Stability/instability can be confirmed by numerical experiment.

We perform a dynamic simulation that starts at a randomly perturbed stable test point *No* 1 on the branch. The result of the numerical experiment is shown in Figure 9 left. Note that we have already assumed the stability of this point by computing the stable/unstable branch segments, see Remark 2.2.

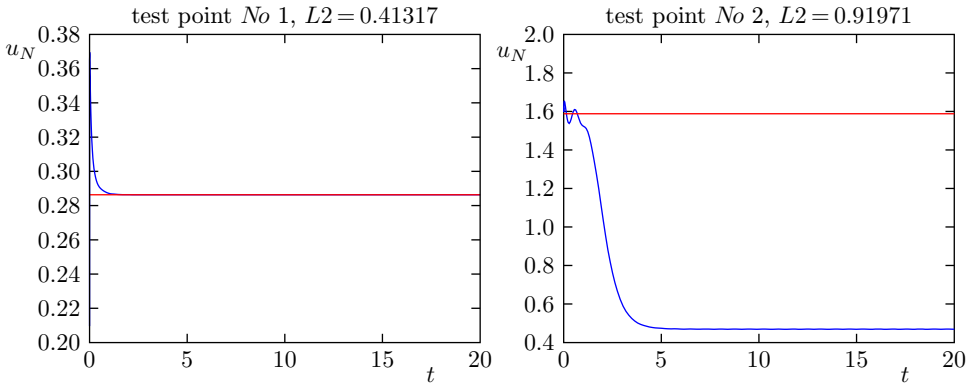

Figure 9. Schnakenberg model, Example 2.1, $N = 40$. Left: Consider the branch $L2\_1\_up$. Dynamic simulation: random perturbation at stable test point *No* 1. Steady state (red), resulting trajectory (blue). Right: Consider the branch $L2\_1\_down$. Dynamic simulation: random perturbation at an unstable test point *No* 2. Steady state (red), resulting trajectory (blue).

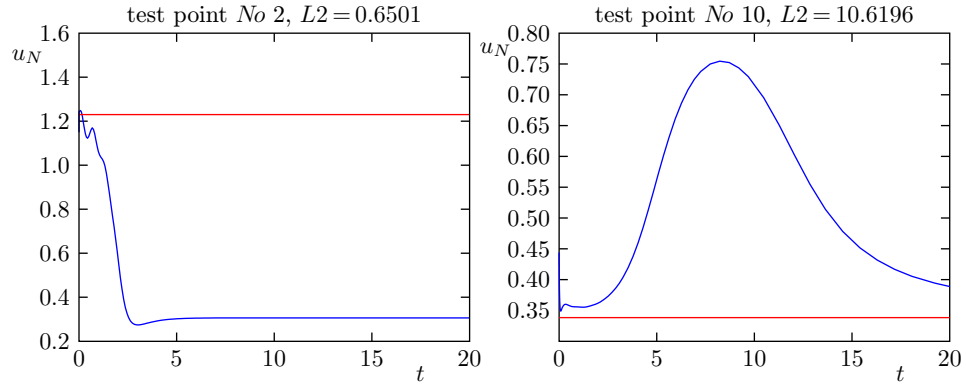

Figure 10. Schnakenberg model, Example 2.1, $N = 40$. Left: Consider the branch $L2\_2\_up$. Dynamic simulation: random perturbation at the unstable test point *No* 2. Steady state (red), resulting trajectory (blue). Right: Consider the branch $L2\_5\_up$. Dynamic simulation: random perturbation at the stable test point *No* 10. Steady state (red), resulting trajectory (blue).

It can be seen from Figure 1 that by performing a dynamic simulation we can reach two steady states.

Consider a randomly perturbed unstable test point *No* 3 on branch $L2\_1\_up$. This is an example that the dynamic simulation may not converge, see Figure 11.

There are unstable steady states in the range $L2\_1\_up < L^2 < L2\_1\_down$. These are the related branches of $L2\_1\_up$ (in Figure 1), and the branches marked as $L2\_2\_up$ and $L2\_1\_down$ (not shown here). We can refer to the global bifurcation diagram in Figure 8. Taking an unstable test point with the ordinate $L^2 = 0.91971$, the dynamic

simulation converges to the stable steady state depicted in Figure 9 right. If we take the unstable test point with the ordinate $L^2 = 0.6501$, the dynamic simulation converges to the stable steady state depicted in Figure 10 left. In principle, the dynamic simulation can only provide stable steady states.

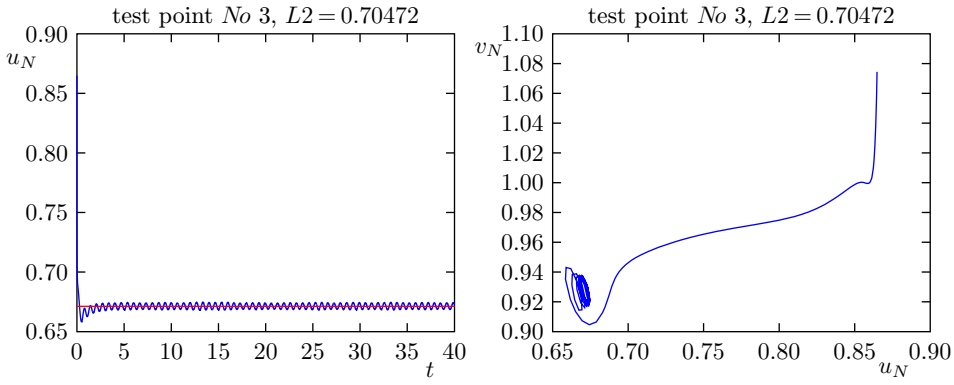

Figure 11. Schnakenberg model, Example 2.1, $N = 40$, the branch *L2_1_up*. Dynamic simulation: random perturbation at the unstable test point *No* 3. Left: Steady state (red), resulting oscillation (blue). Right: Phase portrait of the oscillations.

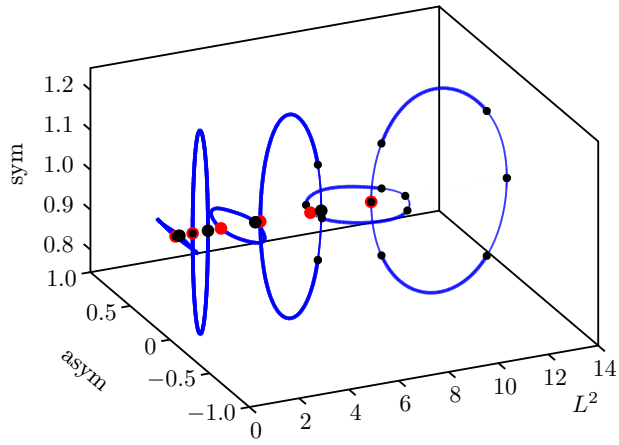

Figure 12. Schnakenberg model, Example 5.1, $N = 40$. Homogeneous steady states are not displayed. Branches of inhomogeneous steady states emanating from *L2_1_up*, *L2_1_down*, *L2_2_up*, *L2_2_down*, *L2_3_up*, *L2_3_down*, *L2_4_up*, *L2_5_up*, *L2_4_down*, *L2_6_up*.

How to recognize the steady state using dynamic simulation? We can usually cut-off transients, see Figure 9 and Figure 10 left. In Figure 10 right, we can observe the *transient growth*, see [12] and [19], Section 14.

Dynamic simulation can be used to investigate the dependence of parameters of the Schnakenberg model. Recall Example 2.1. Let us relax the diffusion parameter d_2 and trace the pairs (3.7). For a critical parameter value $d_2 \approx 0.85$ the continuation breaks down, because we have reached the critical wave number $k_c \approx 34.2$, see Definition 3.1. Choose a parameter d_2 near the critical value $d_2 \approx 0.85$:

Example 5.1. Consider the system (2.19) and set the parameters $a = 0.1$, $b = 0.9$, $\gamma = 10$, $d_1 = 0.1$, $d_2 = 0.9$ and $N = 40$.

Figure 12 shows the relevant bifurcation diagram. Note that the branches *L2_1_up* end *L2_1_down*, *L2_2_up* end *L2_2_down*, *L2_3_up* end *L2_3_down*, *L2_4_up* end *L2_4_down*, respectively, are setwise equal. They differ in parameterization.

Note that the generic scenario in Figure 8 is different from the scenario in Figure 12.

6. Conclusions

The aim of this paper is to promote numerical continuation in solving reaction-diffusion problems. We claim an algorithmic contribution to the continuation algorithm:

(a) branch initialization using Taylor expansion of the bifurcation equation,

(b) branch segmentation by distinguishing stable and unstable segments of the branch.

In principle, we can initialize, compute and sort $2(N-1)$ bifurcation points. Then we can compute the relevant branches using the standard continuation algorithm. The algorithm may collapse due to numerical reasons (too small time step).

We also classified the symmetries of the model. For this purpose, we designed a specific group representation. By concatenating specific branches, we can create a global bifurcation diagram.

This approach has its limits. Unfortunately, the continuation package [5] deals with a single spatial variable. However, considering possible generalizations, we could consider systems with advection [14] or systems for more then two species.

References

[1] *E. L. Allgower, K. Georg*: Introduction to Numerical Continuation Methods. Classics in Applied Mathematics 45. SIAM, Philadelphia, 2003. zbl MR doi

[2] *R. E. Baker, E. A. Gaffney, P. K. Maini*: Partial differential equations for self-organization in cellular and developmental biology. Nonlinearity *21* (2008), R251–R290. zbl MR doi

[3] *K. Böhmer, W. Govaerts, V. Janovský*: Numerical detection of symmetry breaking bifurcation points with nonlinear degeneracies. Math. Comput. *68* (1999), 1097–1108. zbl MR doi

[4] *P. Chossat, R. Lauterbach*: Methods in Equivariant Bifurcations and Dynamical Systems. Advanced Series in Nonlinear Dynamics 15. World Scientific, Singapore, 2000. zbl MR doi

[5] *A. Dhooge, W. Govaerts, Y. A. Kuznetsov*: MATCONT: A MATLAB package for numerical bifurcation analysis of ODEs. ACM Trans. Math. Softw. *29* (2003), 141–164. zbl MR doi

[6] *A. Dhooge, W. Govaerts, Y. A. Kuznetsov*: MATCONT and CL_MATCONT: Continuation Toolboxes in MATLAB. University Gent, Gent, 2011.
[7] *A. Gierer, H. Meinhardt*: A theory of biological pattern formation. Kybernetik *12* (1972), 30–39. zbl doi
[8] *M. Golubitsky, D. G. Schaeffer*: Singularities and Groups in Bifurcation Theory. I. Applied Mathematical Sciences 51. Springer, New York, 1985. zbl MR doi
[9] *M. Golubitsky, I. Stewart, D. G. Schaeffer*: Singularities and Groups in Bifurcation Theory. II. Applied Mathematical Sciences 69. Springer, New York, 1988. zbl MR doi
[10] *W. J. F. Govaerts*: Numerical Methods for Bifurcations of Dynamical Equilibria. SIAM, Philadelphia, 2000. zbl MR doi
[11] *V. Janovský, P. Plecháč*: Numerical applications of equivariant reduction techniques. Bifurcation and Symmetry: Cross Influence Between Mathematics and Applications. International Series of Numerical Mathematics 104. Birkhäuser, Basel, 1992, pp. 203–213. zbl MR
[12] *V. Klika*: Significance of non-normality-induced patterns: Transient growth versus asymptotic stability. Chaos *27* (2017), Article ID 073120, 9 pages. zbl MR doi
[13] *V. Klika, R. E. Baker, D. Headon, E. A. Gaffney*: The influence of receptor-mediated interactions on reaction-diffusion mechanisms of cellular self-organisation. Bull. Math. Biol. *74* (2012), 935–957. zbl MR doi
[14] *V. Klika, M. Kozák, E. A. Gaffney*: Domain size driven instability: Self-organization in systems with advection. SIAM J. Appl. Math. *78* (2018), 2298–2322. zbl MR doi
[15] *Y. A. Kuznetsov*: Elements of Applied Bifurcation Theory. Applied Mathematical Sciences 112. Springer, New York, 1998. zbl MR doi
[16] *A. Marciniak-Czochra, G. Karch, K. Suzuki*: Instability of Turing patterns in reaction-diffusion-ODE systems. J. Math. Biol. *74* (2017), 583–618. zbl MR doi
[17] *J. D. Murray*: Mathematical Biology. II. Spatial Models and Biomedical Applications. Interdisciplinary Applied Mathematics 18. Springer, New York, 2003. zbl MR doi
[18] *J. Schnakenberg*: Simple chemical reaction systems with limit cycle behaviour. J. Theoret. Biol. *81* (1979), 389–400. MR doi
[19] *L. N. Trefethen, M. Embree*: Spectra and Pseudospectra. The Behavior of Nonnormal Matrices and Operators. Princeton University Press, Princeton, 2005. zbl MR
[20] *A. M. Turing*: The chemical basis of morphogenesis. Philos. Trans. R. Soc. Lond., Ser. B, Biol. Sci. *237* (1952), 37–72. zbl MR doi

Author's address: *Vladimír Janovský*, Department of Numerical Mathematics, Faculty of Mathematics and Physics, Charles University, Sokolovská 49/83, 186 75 Praha 8, Czech Republic, e-mail: `janovsky@karlin.mff.cuni.cz`.